

Analysis of a Five-Degree-of-Freedom Hybrid Robot RPR/RP + RR + P



Xuejian Ma, Yundou Xu, Yu Wang, Fan Yang, Yongsheng Zhao, Jiantao Yao, and Yulin Zhou

Abstract This work proposes a hybrid machining robot RPR/RP + RR + P based on a planar parallel mechanism. Based on the screw theory, the characteristics of the degree of freedom of the hybrid robot are analyzed, and then the inverse and forward kinematics are solved by geometric methods. And size optimization is carried out by taking the workspace and driving forces as the objects. Then the working space of the hybrid robot is calculated by the Monte Carlo method. Finally, the three-dimensional model of the mechanism is established, and through ADAMS simulation, the accuracy of the inverse kinematics solution was verified.

Keywords Hybrid machining robot · Inverse kinematics · Forward kinematics · Size optimization · Workspace

X. Ma · Y. Xu (✉) · Y. Wang · F. Yang · Y. Zhao (✉) · J. Yao
Laboratory of Parallel Robot and Mechatronic System of Hebei Province, Yanshan University,
Qinhuangdao 066004, China
e-mail: ydxu@ysu.edu.cn

Y. Zhao
e-mail: yszhao@ysu.edu.cn

J. Yao
e-mail: jtyao@ysu.edu.cn

Y. Xu · Y. Zhao · J. Yao
Key Laboratory of Advanced Forging and Stamping Technology and Science, Yanshan University,
Qinhuangdao 066004, China

X. Ma · Y. Xu · Y. Wang · F. Yang · Y. Zhao · J. Yao · Y. Zhou
School of Mechanical Engineering, Yanshan University, Qinhuangdao 066004, China
e-mail: ylzhou@ysu.edu.cn

1 Introduction

With the development of aerospace, aviation, automotive industries, and so on, the demands for high-efficiency machining of large-scale structural parts with high material removal ratio and complex parts with curved surfaces increase rapidly. At the same time, traditional serial machine tools have insufficient flexibility, large inertia, and parallel machine tools have small working space, which fails to meet the requirements. The new types of machining equipment are urgently needed. Compared with serial robots and parallel robots, hybrid robots combine the advantages of these two robots and have attracted the attention of many researchers and companies. Hybrid robots can be divided into planar hybrid robots (formed by connecting a swing head with a certain degree of freedom (DOF) in serial on a planar parallel mechanism) and spatial hybrid robots (formed by connecting a swing head with a certain DOF in serial on a spatial parallel mechanism). Compared with the spatial hybrid mechanism, the planar hybrid mechanism has the advantages of simple structure, simple kinematics and dynamics models and low manufacturing cost.

At present, there are many spatial hybrid robots, such as Tricept hybrid robots [1, 2], Exechon hybrid machining center [3, 4], TriMule [5, 6] and TriVariant [7, 8] hybrid robots as well as other robots [9–14] etc. And there are relatively few planar hybrid mechanisms. Yang and Wang [15] proposed to develop the XNZD755 planar hybrid machine tool and analyzed the dynamics of the machine tool. A redundantly actuated 3-DOF planar PM was developed in [16] for a 4-DOF hybrid machine tool and again in [17] for 5-DOF one.

This work will propose a new five-DOF planar hybrid robot RPR/RP + RR + P, which is used to machine complex aluminum alloy parts for new energy vehicles.

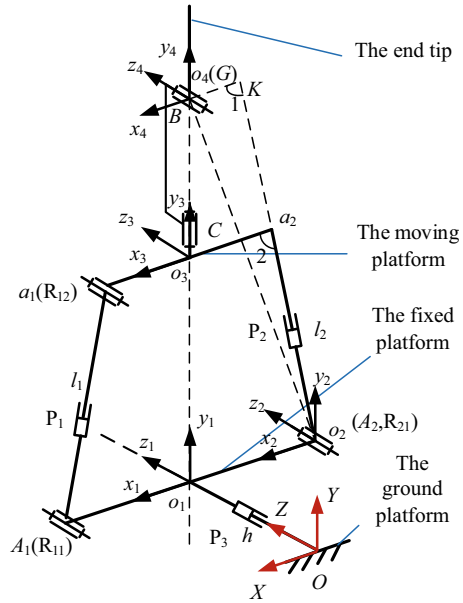
The remainder of this article is organized as follows: Sect. 2 describes the composition of the hybrid robot, and introduces the DOF of the mechanism. Section 3 analyzes the robot's inverse and forward kinematic. Section 4 carries out the size optimization by taking the workspace and driving forces as the objects, and analyzes the workspace of the hybrid robot under the given mechanism parameters. Section 5 gives the three-dimensional model of the mechanism, and the verifies the correction of inverse kinematics analysis. Finally, conclusions are drawn in Sect. 6.

2 Description of the Five-Axis Hybrid Robot

2.1 Mechanism Composition

The RPR/RP + RR hybrid robot proposed in this article is shown in Fig. 1. The robot consists of three parts: a planar parallel mechanism RPR/RP, a serial BC swing head, and a serial P joint. The moving platform of the parallel mechanism RPR/RP is supported by two limbs A_1a_1 and A_2a_2 . The limb A_1a_1 is connected to the fixed platform and moving platform both through the R joint. The limb A_2a_2 is connected

Fig. 1 Schematic diagram of the hybrid robot



to the fixed platform through an R joint, which is connected to the moving platform through a prismatic joint directly. The axes of three R joints are parallel to each other, and the axes of the prismatic are perpendicular to the axes of the R joints.

As shown in Fig. 1, the fixed platform and the moving platform of the parallel mechanism are equivalent to two straight lines. The length of the fixed platform is $2a$, and the length of the moving platform is $2b$. Point G is the intersection point of the BC swing head. The straight-line Go_3 is perpendicular to the moving platform, the vertical foot is the o_2 point, the length of Go_3 is k , and the length between the intersection point of the BC swing head and the tip of the tool is f .

2.2 Coordinate System Establishment

In order to establish the position model of the mechanism, the global frame $O-XYZ$ is established at point O on the fixed platform, where the X -axis is parallel to the line A_2A_1 , the Z -axis is parallel to the axis of the R joint, and the right-hand system rule determines the Y -axis. The local frame $o_1-x_1y_1z_1$ is established at o_1 on the fixed platform, where the x_1 -axis points from point A_2 to A_1 , the z_1 -axis is collinear with the Z -axis, and the right-hand system rule determines the y_1 -axis.

The local frame $o_2-x_2y_2z_2$ is established at point A_2 , where the x_2 -axis is collinear with A_1A_2 , the z_2 -axis is collinear with the axis of the R_{21} , and the right-hand system rule determines the y_2 -axis. The local frame $o_3-x_3y_3z_3$ is established at the midpoint of a_1a_2 , where the x_3 -axis is collinear with a_1a_2 , the y_3 -axis is collinear with the C

axis of the BC swing head, and the right-hand system rule determines the z_3 -axis. Moreover, the local frame $o_4-x_4y_4z_4$ is established at the point G, where the y_4 -axis is collinear with the axis of the end handle, and the z_4 -axis is collinear with the B axis. The right-hand system rule determines the x_4 -axis, as shown in Fig. 1.

2.3 Degree of Freedom Analysis

The hybrid robot is composed of a parallel part and two serial parts. The parallel part mechanism is RPR/RP, composed of limbs A_1a_1 and A_2a_2 . The schematic diagram of the parallel mechanism RPR/RP is shown in Fig. 2.

The DOF of the parallel mechanism can be calculated from the revised G-K formula:

$$K = d(n - g - 1) + \sum_{i=1}^g f_i + v \tag{1}$$

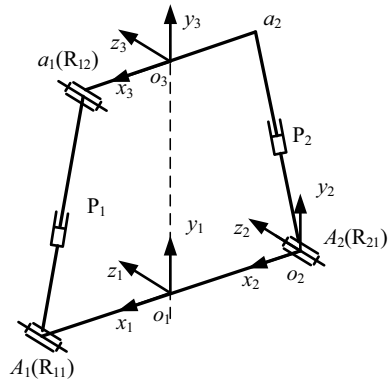
- d The order of the parallel mechanism, $d = 6 - \lambda$;
- n Number of parallel mechanism components;
- g Number of joints of parallel mechanism;
- f_i The number of DOFs of the i th joint;
- v Number of redundant constraints of parallel mechanism.

The expression of redundant constraint v is:

$$v = l - k \tag{2}$$

where l is the number of remaining constraint wrenches after removing the public constraints of the mechanism, and k is the rank of the remaining constraint wrenches.

Fig. 2 Schematic diagram of the parallel mechanism



It can be obtained that l is 3, k is 3, the DOF of the RPR/RP mechanism can be obtained as:

$$\begin{aligned} K &= d(n - g - 1) + \sum_{i=1}^g f_i + v \\ &= 3 \times (5 - 5 - 1) + 5 \\ &= 2 \end{aligned} \quad (3)$$

The DOF of the parallel mechanism is 2, including the translation along the rod A_2a_2 and the rotation around the axis of the R joint at A_2 .

The mechanism is a parallel mechanism in serial with a serial two-DOF BC swing head and a serial one-DOF P joint, so the hybrid robot is a five-DOF hybrid robot.

3 Inverse and Forward Kinematics Analysis

3.1 Inverse Kinematics of Parallel Mechanism

In the inverse solution, it is considered that the coordinates of the tool tip point $\mathbf{F} = [F_x, F_y, F_z]^T$ and the unit direction vector \mathbf{S} of the end tool rod are known, and the purpose is to calculate the input of each actuator, i.e., $h, l_1, l_2, \alpha, \beta$, which are the inputs of P₃, P₁, P₂, C, B respectively.

Because the tool tip point coordinate \mathbf{F} and the unit direction vector \mathbf{S} are known, the coordinates can be easily obtained from the established coordinate system:

$$\begin{aligned} G_x &= F_x - f \cdot [1, 0, 0] \cdot \mathbf{S} \\ G_y &= F_y - f \cdot [0, 1, 0] \cdot \mathbf{S} \\ G_z &= F_z - f \cdot [0, 0, 1] \cdot \mathbf{S} \end{aligned} \quad (4)$$

The expression of point G in the global frame $O-XYZ$ and local frame $o_2-x_2y_2z_2$ can be obtained:

$$\mathbf{G} = (G_x, G_y, G_z)^T \quad \mathbf{G}_2 = (G_x + a, G_y, 0)^T \quad (5)$$

Then the input of P₃ is G_z , that is: $h = G_z$.

As shown in Fig. 1, the angle θ_1 can be obtained by the coordinate relationship of point G in local frame $o_1-x_1y_1z_1$:

$$\begin{aligned} \sin \theta_1 &= \frac{G_x + a}{|G_2|} \\ \cos \theta_1 &= \frac{G_z}{|G_2|} \end{aligned} \quad (6)$$

where θ_1 is the angle of $\angle A_2 G o_1$, l_G is the length of GA_2 .

As shown in Fig. 1, in the trapezoid $GK a_2 o_2$, $\angle 1$ is known, $o_3 a_2 = b$, $Go_3 = k$, then through geometric relations, the length of GK and $K a_2$ can be calculated. In the triangle $GK A_2$, according to the law of sine

$$\sin \theta_2 = \frac{GK \sin(\angle 1)}{|G_2|} \tag{7}$$

where θ_2 is angle of $\angle KA_2 G$.

And the length of l_2 can be calculated based on sine law:

$$l_2 = \frac{GK \sin(\pi - \angle 1 - \theta_2)}{\sin(\theta_2)} - K a_2 \tag{8}$$

After obtaining θ_1 and θ_2 , the rotation angle θ_3 of the mechanism around the axis of R_{21} can be obtained. Then the point of ${}^3 a_i$ ($i = 1, 2$) can be expressed in the local frame $o_1-x_1y_1z_1$.

$${}^1 a_i = R(\theta_3) {}^3 a_i + \frac{1}{3} P \tag{9}$$

where $R(\theta_3)$ is the transformation matrix of local frame $o_3-x_3y_3z_3$ respect to local frame $o_1-x_1y_1z_1$, and $\frac{1}{3} P$ is origin of local frame $o_3-x_3y_3z_3$ respect to local frame $o_1-x_1y_1z_1$, which can be gotten through the closed-loop vector.

The length of two limbs of the parallel part can be obtained:

$$l_i = \|a_{i1} - A_i\| \quad (i = 1, 2) \tag{10}$$

Substituting the coordinates of points a_{11} , a_{21} , A_1 , and A_2 , the length of two limbs can be calculated.

3.2 Solving the Rotational Angles of the Serial Part

The unit direction vector of the hilt is S , $S = (m, n, q)^T$, and set two rotating angles of the BC swing head in the local frame $O-XYZ$: α' is the rotating angle around the x_3 axis, and β' is the rotating angle around the z_4 axis. Then the angle α' and angle β' are:

$$\begin{aligned} \alpha' &= \arctan\left(\frac{n}{m}\right) \\ \beta' &= \arccos(q) \end{aligned} \tag{11}$$

Then through transformation matrix $R(\theta_3)$, the input angle α of head C and the input angle β of head B can be obtained.

3.3 Forward Kinematics Analysis

In the forward solution, the inputs of h , l_1 , l_2 , α and β are known. The purpose is to solve the coordinate $F = [F_x, F_y, F_z]^T$ of the tool tip point and the unit direction vector S of the hilt.

Because the length l_2 is known, the length of l_G can be obtained based on cosine law:

$$l_G = \sqrt{KG^2 + KA_2^2 - 2 \cos(\angle 1) \cdot KG \cdot KA_2} \quad (12)$$

As shown in Fig. 2, in the quadrilateral $A_1A_2a_1a_2$, the length of four sides and $\angle 2$ are known. According to the law of cosines, the length a_1A_1 and the angle of $\angle a_1A_2a_2$ and $\angle a_1A_2A_1$ can be calculated.

According to formula (7), the angle θ_2 can be obtained. Then the angle of $\angle A_1A_2G$ and θ_3 can be obtained by Eq. (13).

$$\begin{aligned} \angle A_1A_2G &= \angle a_1A_2a_2 + \angle a_1A_2A_1 - \theta_2 \\ \theta_3 &= \angle a_1A_2a_2 + \angle a_1A_2A_1 + \angle 1 - \pi \end{aligned} \quad (13)$$

The coordinate of G in the frame $O-XYZ$ can be expressed:

$$G = [l_G \cos(\angle A_1A_2G) - a, l_G \sin(\angle A_1A_2G), h] \quad (14)$$

And the input angles α and β are known, the unit direction vector S can be obtained by the rotation transformation matrix $R(\theta_3)$.

Then the coordinates of the tool tip point F can be obtained.

$$\begin{aligned} F_x &= G_x + f \cdot [1, 0, 0] \cdot \vec{S} \\ F_y &= G_y + f \cdot [0, 1, 0] \cdot \vec{S} \\ F_z &= G_z + f \cdot [0, 0, 1] \cdot \vec{S} \end{aligned} \quad (15)$$

4 Dimensional Optimization and Workspace Analysis

Taking the working space and driving force as optimization objective, the robot's key dimensions are optimized. The parallel mechanism part is optimized as the main optimization object of the hybrid robot. Firstly, the parallel mechanism is determined based on the size of the BC swing head, and the size of its moving platform is 420 mm. Secondly, based on the limit of the drive joint, the change range of the PM's limb is determined to be [390 mm, 760 mm], and the optimization range of the fixed

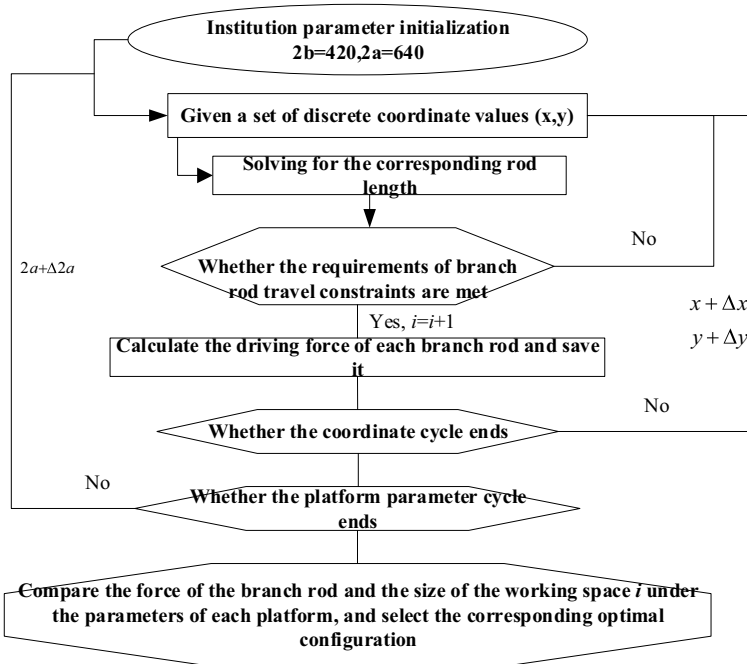


Fig. 3 Flow chart of platform parameter scaling optimization

platform's size is [640 mm, 840 mm]. Under the action of external force $F = [10 \text{ N}, 10 \text{ N}, 10 \text{ N}, 10 \text{ N mm}, 10 \text{ N mm}, 10 \text{ N mm}]^T$, finding the optimal size of the fixed platform through optimization. The flow chart of the optimization procedure is shown in Fig. 3. Table 1 lists the force and workspace indexes with different sizes of the fixed platform.

Finally, through comparison, it is determined that the fixed platform size of the parallel mechanism is 740 mm. Therefore, the key dimensions of the hybrid robot are shown in Table 2.

According to the dimensions given in Table 2, the Monte Carlo method is used to analyze the new workspace of the hybrid robot, and its dexterity space is shown in Fig. 4.

Through observation, the robot can translate in a large range in the Z direction, which is convenient for machining narrow and long parts. At the same time, due to the existence of the BC swing head, the flexibility of the robot end tool in the workspace can be ensured, which is convenient for machining various complex curved surfaces, holes, etc. Therefore, it can meet the machining workspace requirements of aluminum alloy parts with complex curved surfaces for new energy vehicles.

Table 1 The force and workspace indexes with different sizes of the fixed platform

Fixed platform size (mm)	The average value of limb 1 driving force (N)	The average value of limb 2 driving force (N)	Average value of the difference in driving force between limbs 1 and 2 (N)	Driving force fluctuation coefficient of limb 1	Driving force fluctuation coefficient of limb 2	Driving force difference fluctuation coefficient of limbs 1 and 2	Workspace (points)
640	19.2932	30.6320	11.3388	1.5627	1.9477	0.4247	142,618
660	18.3576	29.6661	11.3085	1.2791	1.7073	0.4689	139,208
680	17.4987	28.7601	11.2613	1.0499	1.5217	0.5154	136,055
700	16.7077	27.9063	11.1986	0.8619	1.3777	0.5647	133,149
720	15.9776	27.0992	11.1216	0.7079	1.2676	0.6172	130,466
740	15.3024	26.3337	11.0313	0.5833	1.1846	0.6734	127,986
760	14.6774	25.6062	10.9288	0.4860	1.1235	0.7329	125,710
780	14.0981	24.9141	10.8160	0.4167	1.0784	0.7933	123,518
800	13.5609	24.2544	10.6936	0.3762	1.0464	0.8551	121,453
820	13.0622	23.6249	10.5627	0.3639	1.0244	0.9174	119,482
840	12.5988	23.0233	10.4244	0.3750	1.0095	0.9792	117,553

Table 2 The key dimensions of hybrid robot RPR/RP + RR

Symbol	Value	Symbol	Value
a	370 mm	l_{1max}, l_{2max}	760 mm
b	210 mm	l_{1min}, l_{2min}	390 mm
k	424.5 mm	h_{min}, h_{max}	[0, 2000] mm
f	200 mm	α	[- 180°, 180°]
$\angle 1$	114.567°	β	[- 90°, 90°]

5 Simulation Verification of Inverse Kinematic Analysis

Based on the obtained dimensions of the hybrid robot RPR/RP + RR + P shown in Table 2. As shown in Fig. 5, the three-dimensional model of the hybrid robot RPR/RP + RR + P is designed.

In ADAMS, a motion trajectory is given for the tool tip of the hybrid robot, as shown in Eq. (16).

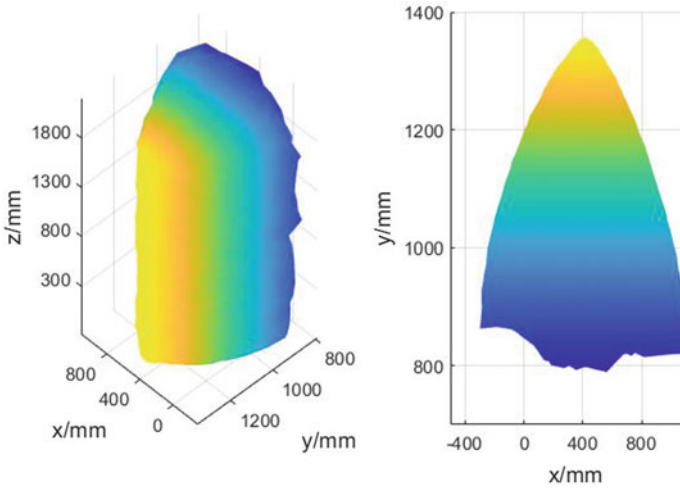
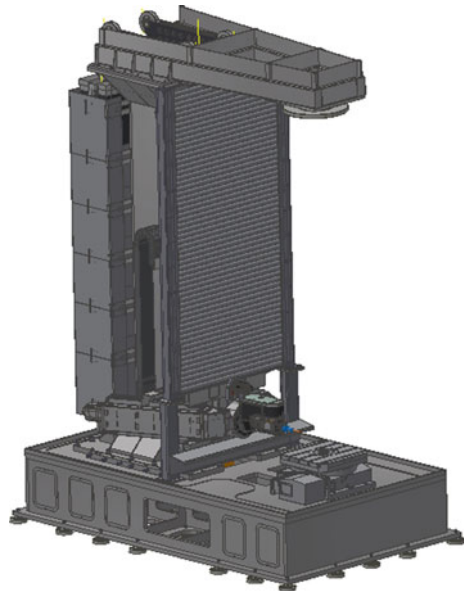


Fig. 4 The workspace of the five-axis hybrid robot RPR/RP + RR + P

Fig. 5 Three-dimensional model of the hybrid robot



$$\begin{cases} X = 20t \text{ (mm)} & t \in [1, 5] \\ Y = 10(t - 5) \text{ (mm)} & t \in [5, 10] \\ Z = 40t \text{ (mm)} & t \in [1, 5] \\ \alpha' = \pi t / 45 \text{ (}^\circ\text{)} & t \in [1, 5] \\ \beta' = \pi t / 90 \text{ (}^\circ\text{)} & t \in [1, 5] \end{cases} \tag{16}$$

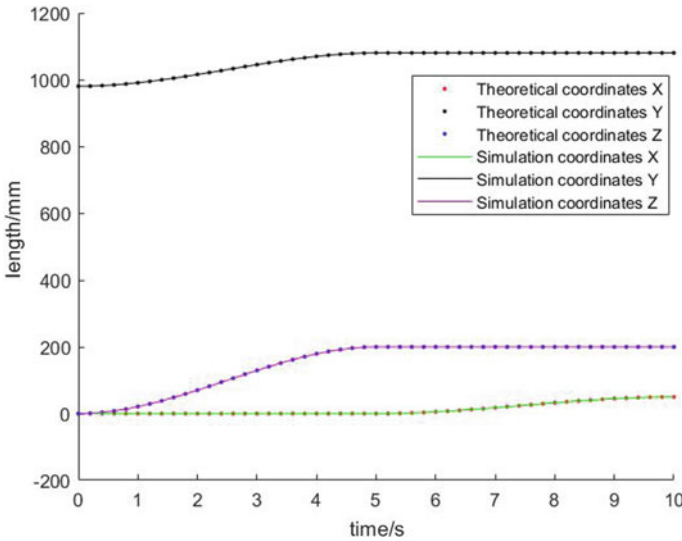


Fig. 6 The coordinates variation curve of end tip measured in the simulation model

After simulation, the lengths l_1 , l_2 , h , and angles α , β of the BC swing head can be measured. Then substituting the inputs into forward kinematics model, the coordinate curve of the tool tip can also be obtained again, as shown in Fig. 6. It can be found that the results are consistent with the values given by Eq. (16), indicating the kinematics analysis is correct.

6 Conclusions and Future Works

A new type of five-degree-of-freedom hybrid robot RPR/RP + RR + P is proposed for machining of aluminum alloy plates for new energy vehicles. The modified hybrid robot includes a two-degree-of-freedom parallel mechanism and two series parts, which are the translation along the limb A_2a_2 and the rotation around the axis of the R joint.

Through the screw theory, the degree of freedom of the robot is analyzed, and the result shows that the robot has five DOFs, and can achieve five-axis hybrid processing.

Through the geometric relationship, the forward and inverse position solutions of the hybrid robot are analyzed. Compared with the general hybrid robot, the forward and inverse position model are simple, thus the hybrid robot is easy to control.

Taking the limb driving forces and working space as the optimization objective, the dimensions of the mechanism is optimized, and the fixed platform size is determined

to be 370 mm. After that, the working space of the robot is obtained by the Monte Carlo method, which is a cylindrical body with an approximate triangular section.

Finally, the three-dimensional model of the mechanism is also constructed through Solidworks software, and the forward and inverse kinematic models of the hybrid robot are verified by using the software ADAMS and MATLAB.

The force and stiffness analysis of the five-axis hybrid machining robot will be carried out in future work. And the prototype will be developed, the prototype experiments will be carried out.

Acknowledgements Supported by the National Natural Science Foundation of China (Grant No. 51875495), and the National Natural Science Foundation of China (Grant No. U2037202), and Hebei Science and Technology Project (Grant No. 206Z1805G).

References

1. Caccavale F, Siciliano B, Villani L (2003) The Tricept robot: dynamics and impedance control. *IEEE/ASME Trans Mechatron* 8(2):263–268
2. Neumann KE (2004) Next generation Tricept—a true revolution in parallel kinematics. In: *Proceedings of the 4th Chemnitz parallel kinematics seminar*, pp 591–594
3. Zhao YQ, Jin Y, Zhang J (2016) Kinetostatic modeling and analysis of an Exechon parallel kinematic machine (PKM) module. *Chin J Mech Eng* 29(1):33–44
4. Jin Y, Bi ZM, Liu HT et al (2015) Kinematic analysis and dimensional synthesis of Exechon parallel kinematic machine for large volume machining. *J Mech Robot* 7(4):041004
5. Huang T, Dong C, Liu H et al (2019) A simple and visually orientated approach for type synthesis of over-constrained 1T2R parallel mechanisms. *Robotica* 37(7):1161–1173
6. Huang T, Cheng LD, Liu H et al (2018) Five-degree-of-freedom hybrid robot with rotational supports. U.S. Patent, 17 Apr 2018
7. Li M, Huang T, Chetwynd DG et al (2006) Forward position analysis of the 3DOF module of the TriVariant: a 5DOF reconfigurable hybrid robot. *J Mech Des* 128(1):319–322
8. Wang YY, Huang T, Zhao XM et al (2007) Finite element analysis and comparison of two hybrid robots—the Tricept and the TriVariant. In: *IEEE/RSJ international conference on intelligent robots and systems*, pp 490–495
9. Liu XJ, Wang LP, Xie F, Bonev IA (2010) Design of a three-axis articulated tool head with parallel kinematics achieving desired motion/force transmission characteristics. *ASME J Manuf Sci Eng* 132(2):021009
10. Xie FG, Liu XJ, Wang JS (2012) A 3-DOF parallel manufacturing module and its kinematic optimization. *Robot Comput Integr Manuf* 28:334–343
11. Li QC, Hervé JM (2014) Type synthesis of 3-DOF RPR-equivalent parallel mechanisms. *IEEE Trans Robot* 30(6):1333–1343
12. Zhang DS, Xu YD, Yao JT, Zhao YS (2019) Analysis and optimization of a spatial parallel mechanism for a new 5-DOF hybrid serial-parallel manipulator. *Chin J Mech Eng* 31(1)
13. Xu YD, Zhang DS, Yao JT, Zhao Y (2017) Type synthesis of the 2R1T parallel mechanism with two continuous rotational axes and study on the principle of its motion decoupling. *Mech Mach Theory* 108:27–40
14. Xu Y, Yang F, Xu Z, Yao J, Zhou Y, Zhao Y (2020) TriRhino: a five-DOF hybrid serial-parallel manipulator with all rotating axes being continuous: stiffness analysis and experiments. *ASME J Mech Robot* 11:23
15. Yang Y, Wang LP (2005) Inverse dynamics analysis of a new type of parallel machine tool. *Tool Technol* 06:11–13

16. Wu J, Wang J, Wang L, Li T (2009) Dynamic and control of a planar 3-DOF parallel manipulator with actuation redundancy. *Mech Mach Theory* 44:835–849
17. Wang L, Wu J, Wang J, You Z (2009) An experimental study of a redundantly actuated parallel manipulator for a 5-DOF hybrid machine tool. *IEEE/ASME Trans Mechatron* 14(1):72–81